Am J Transl Res 2019;11(8):4776-4788
www.ajtr.org /ISSN:1943-8141/AJTR0093973

Original Article

CircPOMT1 and circMCM3AP inhibit osteogenic differentiation of human adipose-derived stem cells by targeting miR-6881-3p

Xin-Qi Huang[1,2*], Xiao Cen[1,3*], Wen-Tian Sun[1,2], Kai Xia[1,2], Li-Yuan Yu[1,2], Jun Liu[1,2#], Zhi-He Zhao[1,2#]

[1]State Key Laboratory of Oral Diseases & National Clinical Research Center for Oral Diseases, West China Hospital of Stomatology, Sichuan University, No. 14, 3rd Section, South Renmin Road, Chengdu 610041, Sichuan, China; [2]Department of Orthodontics, West China Hospital of Stomatology, Sichuan University, Chengdu, China; [3]Department of Temporomandibular Joint, West China Hospital of Stomatology, Sichuan University, Chengdu, China. [*]Equal contributors and co-first authors. [#]Equal contributors.

Received March 17, 2019; Accepted July 7, 2019; Epub August 15, 2019; Published August 30, 2019

Abstract: Circular RNAs (circRNAs), novel endogenous non-coding RNAs with the special circular structure, have been found to play critical roles in various development of tissues and diseases. However, few studies have focused on the functions and mechanisms of circRNAs in the osteogenesis of human adipose-derived stem cells (hASCs). Here, we performed the circRNAs sequencing and bioinformatic analysis to investigate the expression profiles of hASCs during osteogenic differentiation. There were 150 upregulated circRNAs and 60 downregulated circRNAs expressed differentially. Among them, the expression of circPOMT1 and circMCM3AP were downregulated during the osteogenesis of hASCs. hsa-miR-6881-3p could promote the osteogenic differentiation of hASCs, while the expression of circPOMT1 and circMCM3AP were negatively correlated with it. Smad6 and Chordin, critical inhibitors of the BMPs signaling pathway, were predicted to be the targets of hsa-miR-6881-3p. Therefore, circPOMT1 and circMCM3AP might influence the osteogenic differentiation of hASCs by targeting hsa-miR-6881-3p via BMPs signaling pathway. CircPOMT1 and circMCM3AP are potential novel targets for the repairment of bone defects.

Keywords: circPOMT1, circMCM3AP, miR-6881-3p, osteogenic differentiation, hASCs

Introduction

Bone defects, which are caused by trauma, tumor surgery, and inflammation, affect the quality of life of patients seriously and remain a major clinical challenge [1]. Bone tissue engineering is expected to become a new way to repair bone defects [2]. Human adipose-derived stem cells (hASCs), which are derived from adipose tissue, are capable of self-renewal and multilineage differentiation. Owing to the advantages of few side effects and low immunogenic properties, hASCs have been considered as favorable seed cells for bone regeneration [3, 4]. They were involved in the repairment of craniofacial injuries and humerus fractures [5, 6], and the regeneration of tendons, muscles, and cartilage [7, 8]. However, the specific mechanism at the molecular and genetic levels of osteogenic differentiation of hASCs is still unclear, which is the core issue and crucial information in bone tissue engineering.

Circular RNAs (circRNAs), one kind of novel endogenous non-coding RNAs, contained a covalently closed ring structure which was generated by splicing during the maturation of pre-mRNAs [9, 10]. This special circular structure without 5' and 3' ends enables circRNAs to be more stable and resistant to RNase R [11]. According to basic components, circRNAs can be divided into three patterns, including exonic circRNAs, intronic circRNAs, and exon-intron circRNAs [12, 13].

Recent studies have revealed that circRNAs were involved in gene regulation during the transcriptional and posttranscriptional stages [14]. CircRNAs could combine with the RNA-binding protein to regulate the expression of targeted genes [11], and circRNAs also consist of the internal ribosome-entry site, which is conducive to the translation of the effective protein [15, 16]. In addition, circRNAs can serve as the competitive endogenous RNAs to sponge

microRNAs (miRNAs) efficiently, weakening or eliminating the inhibitive effect of miRNAs on the target genes, and regulating the protein synthesis accordingly [10, 14, 17]. The rapidly developing high throughput sequencing technique has broadened the knowledge of circRNAs, demonstrating that they were widely expressed and distributed in the eukaryotic transcriptome [18-20] and participated in the embryonic development, cellular activities, and the development of a variety of human diseases [21, 22], acting as the potential biomarkers of the precise treatments, including neural development [23], cancers [24], wound healing [25], liver regeneration [26], and cardiovascular diseases [27, 28]. However, the effects of the circRNAs on the osteogenic differentiation of hASCs remain unclear.

In this study, we investigated the expression profiles of hASCs during osteogenic differentiation by the circRNAs sequencing and bioinformatic analysis. Two novel circRNAs, namely circPOMT1 and circMCM3AP, were identified, which might inhibit the osteogenesis of hASCs. Then we found hsa-miR-6881-3p, which interacted with circPOMT1 and circMCM3AP, could promote the osteogenic differentiation of hASCs via BMPs signaling pathway. Our results laid the foundation for the future studies to investigate the roles of circRNAs in the osteogenesis of hASCs and utilize it to repair the bone defects more safely and efficiently.

Materials and methods

Cell culture and osteogenic differentiation

The hASCs were purchased from Cyagen company (Guangzhou, China). They were maintained in the OriCell™ general medium which contained 10% fetal bovine serum (FBS), 1% glutamine, and 1% penicillin-streptomycin. The hASCs in the control group (CG) were cultured in this general medium. Osteogenic differentiation of hASCs was induced after 80% confluence. The hASCs in the osteogenic group (OG) were cultured with osteogenic inductive media, which consisted of basic medium supplemented with 10 nM dexamethasone, 50 μg/ml vitamin C, and 10 mM β-glycerophosphate (Sigma-Aldrich, St. Louis, MO, USA). All the cells were cultured in an incubator under 5% CO_2 at 37°C.

Alizarin red s (ARS) staining

ARS staining was designed to visualize the mineral deposition to identify the osteogenic differentiation of hASCs. The samples were rinsed with phosphate buffered saline (PBS) 3 times and fixed in 4% paraformaldehyde solution for 20 minutes. They were stained with 0.1% ARS (pH = 4.2) for 20 minutes at 25°C.

Alkaline phosphatase (ALP) staining and ALP activity

ALP staining was performed by the Alkaline Phosphatase Assay Kit (Beyotime, China) according to the manufacturer's instruction. Briefly, hASCs were rinsed with PBS and fixed in in citrate solution for 30 seconds. Then hASCs were stained with a solution of FRV alkaline, sodium nitrite, and naphthol AS-BI alkaline for 15 min away from light.

For the ALP activity analysis, the cultured cells were rinsed 3 times with PBS, followed by 1% Triton X-100. Then they were scraped into distilled water. The ALP activity was quantified at 405 nm using p-nitrophenyl substrate.

CircRNAs sequencing

Total RNAs were extracted from the hASCs with the Trizol reagent (Invitrogen, Carlsbad, CA, USA) according to the manufacturer's protocol. The purity and concentration of each RNAs sample were determined by NanoDrop ND-1000 (NanoDrop Thermo, Wilmington, DE, USA) on basis of a qualified ratio of OD260 to OD-280 (1.8~2.1). RNAs integrity was detected by 1% formaldehyde denaturing gel electrophoresis. For each sample, 5 μg of total RNAs was treated with 3 units/μg of RNase R (Epicentre, Inc., Madison, WI, USA) for 15 min at 37°C to remove linear RNAs. Ribo-Zero Magnetic Gold Kit (Epicentre, Inc., Madison, WI, USA) was applied to deplete rRNAs of the RNase-R treated RNAs.

CircRNAs sequencing and RNAs library construction were completed by CloudSeq Biotech Inc. (Shanghai, China). The RNAs libraries were constructed by the rRNAs-depleted RNAs with TruSeq Stranded Total RNAs Library Prep Kit (Illumina, San Diego, CA, USA). The library quality was determined by BioAnalyzer 2100 system (Agilent Technologies, Inc., Richardson, TX,

USA). RNAs-Seq library sequencing was performed on the Illumina HiSeq platform (San Diego, CA, USA). Then the raw data were filtered to clear the low-quality reads.

Bioinformatic analysis

To investigate the profiling of differentially expressed circRNAs, the hierarchical clustering analysis was conducted on basis of the expression levels of all identified circRNAs by Cluster and TreeView software, which showed the significant differences between OG and CG. The functions of the differentially expressed circRNAs between these two groups were predicted by Gene ontology (GO) and Kyoto Encyclopedia of Genes and Genomes (KEGG) pathways analyses. The interaction networks of circRNAs-miRNAs-mRNAs were predicted by miRanda and presented with Cytoscape software (v2.8.0).

Transfection of mimic and inhibitor

The RNA oligoribonucleotides used in present study, including hsa-miR-6881-3p mimic, hsa-miR-6881-3p inhibitor, si-circPOMT1, si-circMCM3AP, and corresponding negative controls were synthesized by GenePharma Co. (Shanghai, China). The cells were seeded 2×10^5 per well on 24-well plates and cultured with general medium. They were transfected by Lipofectamine 3000 Reagent (Invitrogen, Carlsbad, USA) when reaching 70% confluency. The primers of these RNA oligoribonucleotides are listed in Table S1.

RNA isolation and quantitative real-time PCR (qRT-PCR)

For circRNAs validation, total RNAs (3 μg) were used for cDNA synthesis with dNTP Mix (HyTestLtd, Turku, Finland), SuperScript III Reverse Transcriptase (Thermo Fisher Scientific, Chino, CA, USA), and RNase inhibitor (Enzymatics, GreenBay, Wisconsin, USA). qRT-PCR was performed in ViiA 7 Real-time PCR System (Applied Biosystems, Wilmington, DE, USA) with SYBR Green master mix (Cloudseq, Shanghai, China).

For mRNAs detection, 500 ng of total RNAs were used for DNA synthesis with a PrimeScript RT reagent kit (Takara Bio, Inc.). qRT-PCR was performed in triplicate with SYBR Premix Ex Taq (Takara Bio, Inc.). Expression data were normalized to β-ACTIN. The primers were designed by Sangon (Shanghai, China) (Table S2).

The miRNA qRT-PCR Detection Kit (GeneCopoeia) was used for both cDNA synthesis and quantitative detection using miR-6881-3p-specific primers (GeneCopoeia). U6 was used for normalization. All the relative target genes expression was calculated by the formula $2^{-\Delta\Delta Ct}$.

Western blot

Total cell protein was extracted using radio immunoprecipitation assay (RIPA) lysis buffer. The protein concentration was measured by the BCA protein assay kit (Thermo, USA). Equal numbers of protein were separated by sodium dodecyl sulfate-polyacrylamide gel electrophoresis (SDS-PAGE), and then transferred onto PVDF membranes (Millipore, USA). The PVDF membranes were incubated overnight at 4°C with primary antibodies against anti-RUNX2 (1:1000, CST, USA), anti-OPN (1:1000, Huabio, China), and β-ACTIN (1:1000, Huabio, China). After washed 3 times with TBST, the membranes were incubated with corresponding secondary antibodies (1:10000, Invitrogen, USA) for 2 h. The band intensity was quantified by ImageJ software. Each target band was normalized to β-ACTIN band.

Statistical analysis

Quantitative data were presented as means ± standard deviation (SD) from at least 3 independent experiments. One-way analysis of variance (ANOVA) was employed for multiple group testing, while differences between two groups were evaluated by t-test. The two-tailed $P < 0.05$ was considered as statistical significance. The statistical calculations were performed with SPSS 17.0 software (SPSS Inc., Chicago, IL).

Results

Osteogenic differentiation of hASCs

After induced for 7 days, the intensity of ALP staining was significantly stronger in OG than CG (**Figure 1A**). The quantification of ALP activity was also higher in OG than CG, which was in coincidence with the ALP staining (**Figure 1B**).

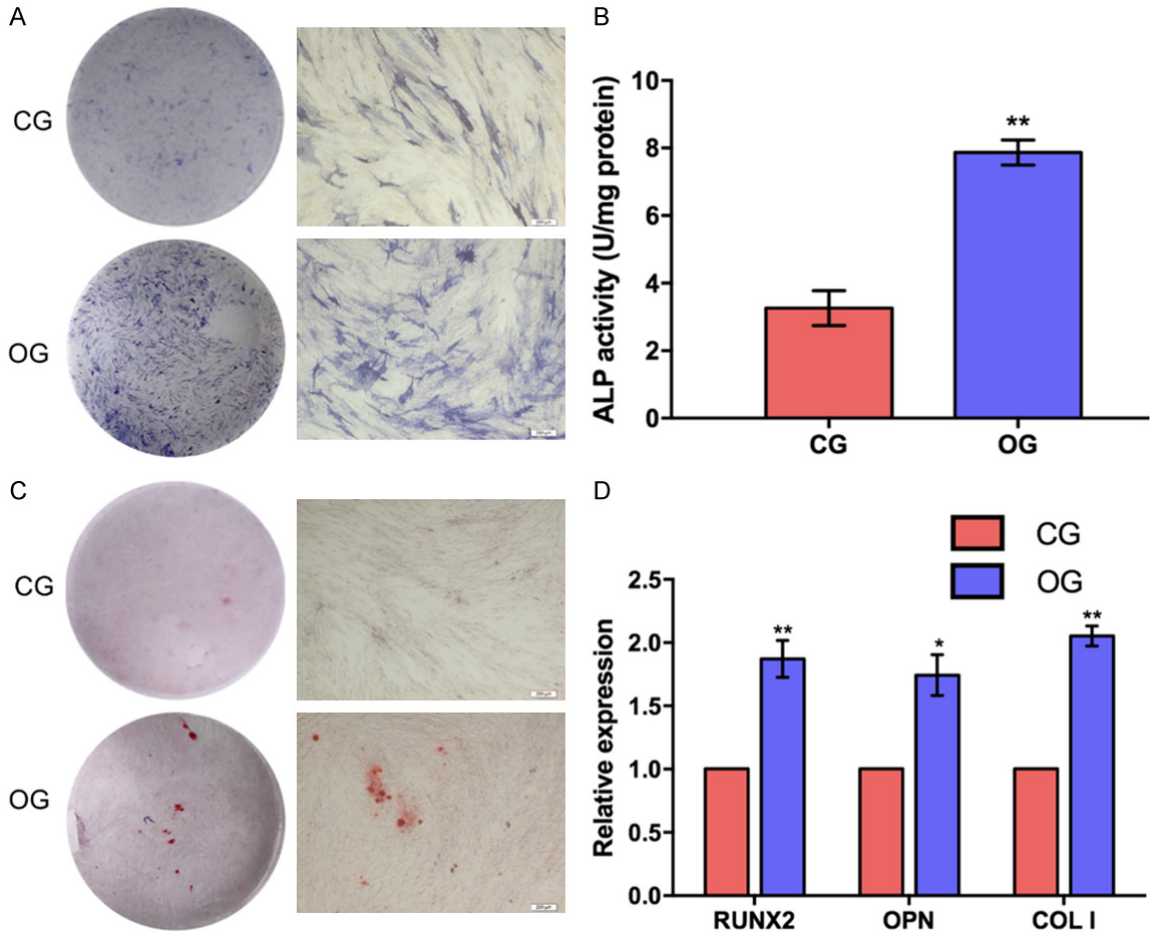

Figure 1. The osteogenic differentiation of hASCs. A. The ALP staining confirmed the successful osteogenic differentiation of hASCs in OG (scale bar = 200 um). B. Quantification of ALP activity showed stronger ALP activity in OG than that in CG. C. The ARS staining of hASCs confirmed the successful osteogenesis of hASCs in OG (scale bar = 200 um). D. Real-time qPCR showed the genes related to osteogenesis were upregulated significantly in OG (*, $P < 0.05$, **, $P < 0.01$).

The calcified nodules of ARS staining were apparently spotted in OG, while the intensity of ARS staining was weaker significantly in CG than in OG (**Figure 1C**). The mRNA expression levels of RUNX2, OPN, and COL I were upregulated in OG significantly, compared with those in CG (**Figure 1D**).

Expression profiles of circRNAs during osteogenesis of hASCs

The overall comparison of differentially expressed circRNAs was presented by the heatmap (**Figure 2A**). There were 210 circRNAs expressed differentially significantly (p-value < 0.05, fold-change > 2). Each dot stood for a circRNA in the volcano plot. The red dots on the left side stood for the downregulated circRNAs and those on the right side stood for the upregulated circRNAs with significant differences, while the grey dots stood for the circRNAs which expressed differentially without significance, that is, 150 circRNAs were upregulated and 60 circRNAs were downregulated significantly (**Figure 2B**).

Six differentially expressed circRNAs, circUSP53, circZBTB16, circXLOC_007414, circTIPARP, circMCM3AP, and circPOMT1, were selected based on their P value, fold change, and raw intensity. When compared with those in CG, the expression levels of circUSP53, circZBTB16, circXLOC_007414, and circTIPARP were increased in OG, while the expression levels of circMCM3AP and circPOMT1 were decreased. These results corresponded to the qRT-PCR data (**Figure 2C**).

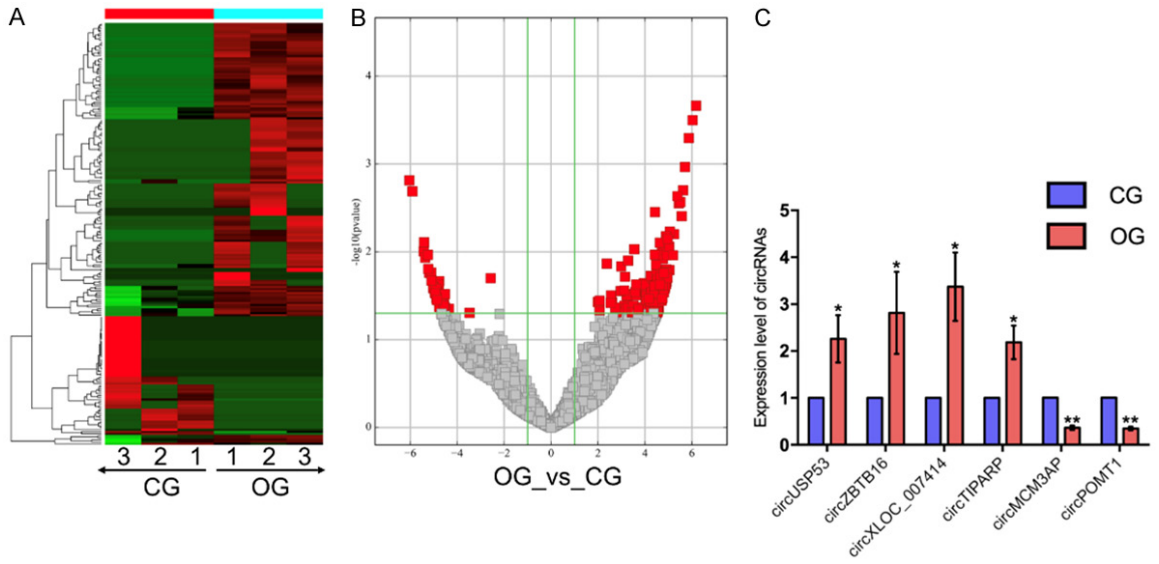

Figure 2. Expression profiles of circRNAs during osteogenic differentiation. A. The overall expression of circRNAs were displayed in the heatmap. B. Volcano plot showed that 60 circRNAs were downregulated and 150 circRNAs were upregulated during osteogenesis. C. Real-time qPCR showed that CircUSP53, circZBTB16, circXLOC_007414, and circTIPARP were significantly upregulated, while circMCM3AP and circPOMT1 were downregulated in OG (*, $P < 0.05$, **, $P < 0.01$).

Functional analysis of the parental genes of circRNAs

The GO analysis for the parental genes of differentially expressed circRNAs consisted of three parts, including biological processes (BP), cellular components (CC), and molecular function (MF). The top 60 enrichment GO analysis was displayed in **Figure 3A**. The most enriched BP terms were associated with positive regulation of hydrolase activity (GO: 0051345), regulation of GTPase activity (GO: 0043087), and positive regulation of GTPase activity (GO: 0043547). As for CC, the most enriched terms were concerned with adherence junction (GO: 0005912), anchoring junction (GO: 0070161), and cell leading edge (GO: 0031252). The most enriched MF terms were related to small GTPase binding (GO: 0031267), GTPase binding (GO: 0051020), and Ras GTPase binding (GO: 0017016).

Regarding the KEGG pathway analysis, the top 41 pathways were listed based on their enrichment scores (**Figure 3B**). Three pathways were indicated to be the most enriched pathways, namely Prostate cancer (hsa05215), Shigellosis (hsa05131), and Bacterial invasion of epithelial cells (hsa05100).

Characterization and confirmation of circPOMT1 and circMCM3AP

CircPOMT1 and circMCM3AP were downregulated in OG compared to CG, which was validated by the qRT-PCR (**Figure 4A**). After treated with RNase R, the expression of circPOMT1 and circMCM3AP remained detectable, which confirmed the existence of a closed-loop structure in these two circRNAs.

PANTHER pathway analysis displayed the related signaling pathways based on the predicted data, demonstrating that circPOMT1 and circMCM3AP might interact with PI3K-Akt signaling pathway, transcriptional mis-regulation in cancer, and Rap1 signaling pathway (**Figure 4B**).

CircPOMT1 and circMCM3AP co-targeted hsa-miR-6881-3p

The circRNAs-miRNAs-mRNAs network, consisting of circPOMT/circMCM3AP with co-targeted miRNAs and mRNAs, was predicted based on miRanda and mapped by Cytoscape (**Figure 4C**). Venn Diagram showed that circPOMT1 and circMCM3AP co-targeted 4 miRNAs, including hsa-miR-29a-3p, hsa-miR-29b-3p, hsa-miR-29c-3p, and hsa-miR-6881-3p (**Figure 5A**). Based on the prediction results of

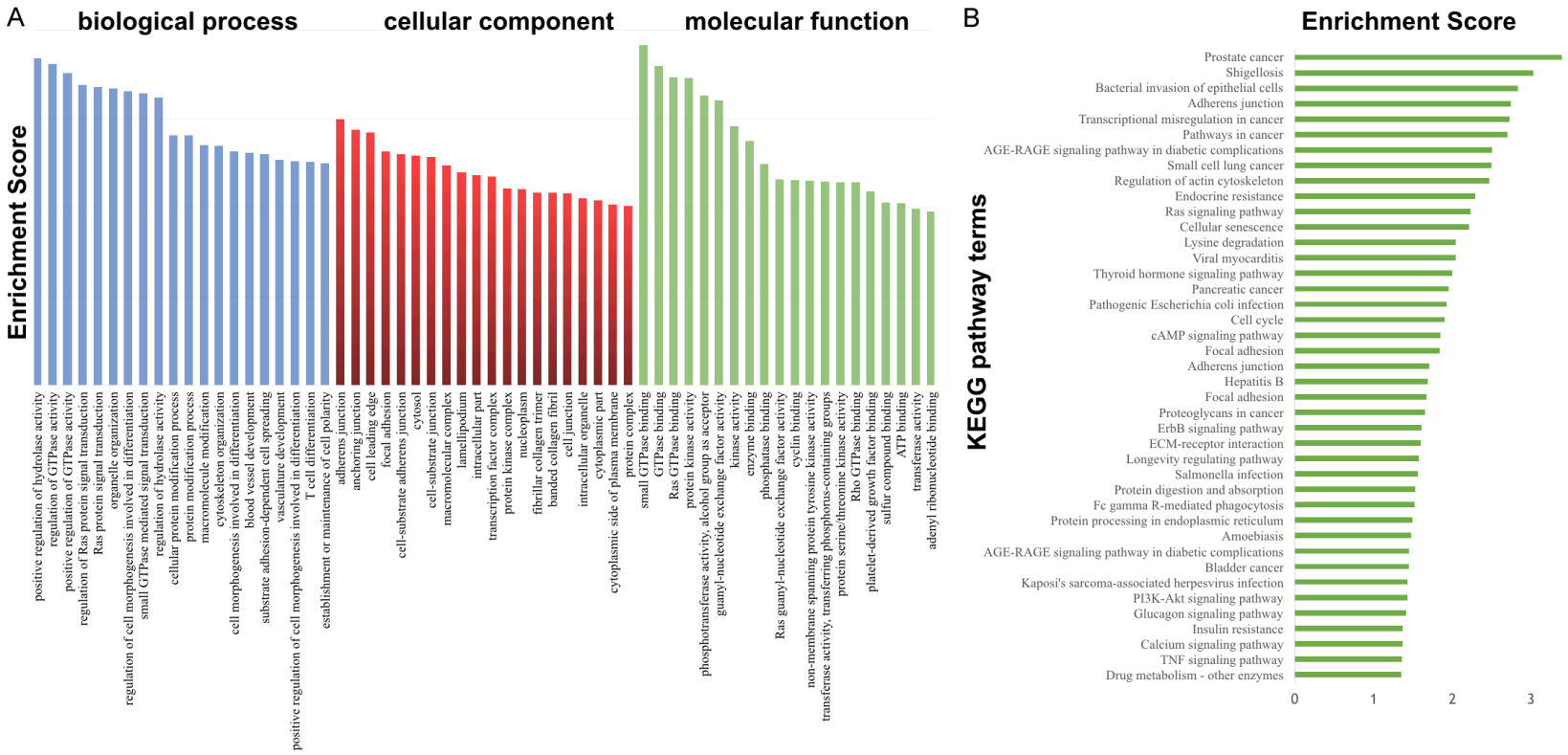

Figure 3. Functional analysis of the parental genes of circRNAs. A. GO annotations ($P < 0.05$) included the top 60 parental mRNAs, involving biological processes, cellular components, and molecular functions. B. KEGG pathway analysis of parental mRNAs showed the top 41 mRNA-enriched pathways, including Prostate cancer, Shigellosis, and Bacterial invasion of epithelial cells.

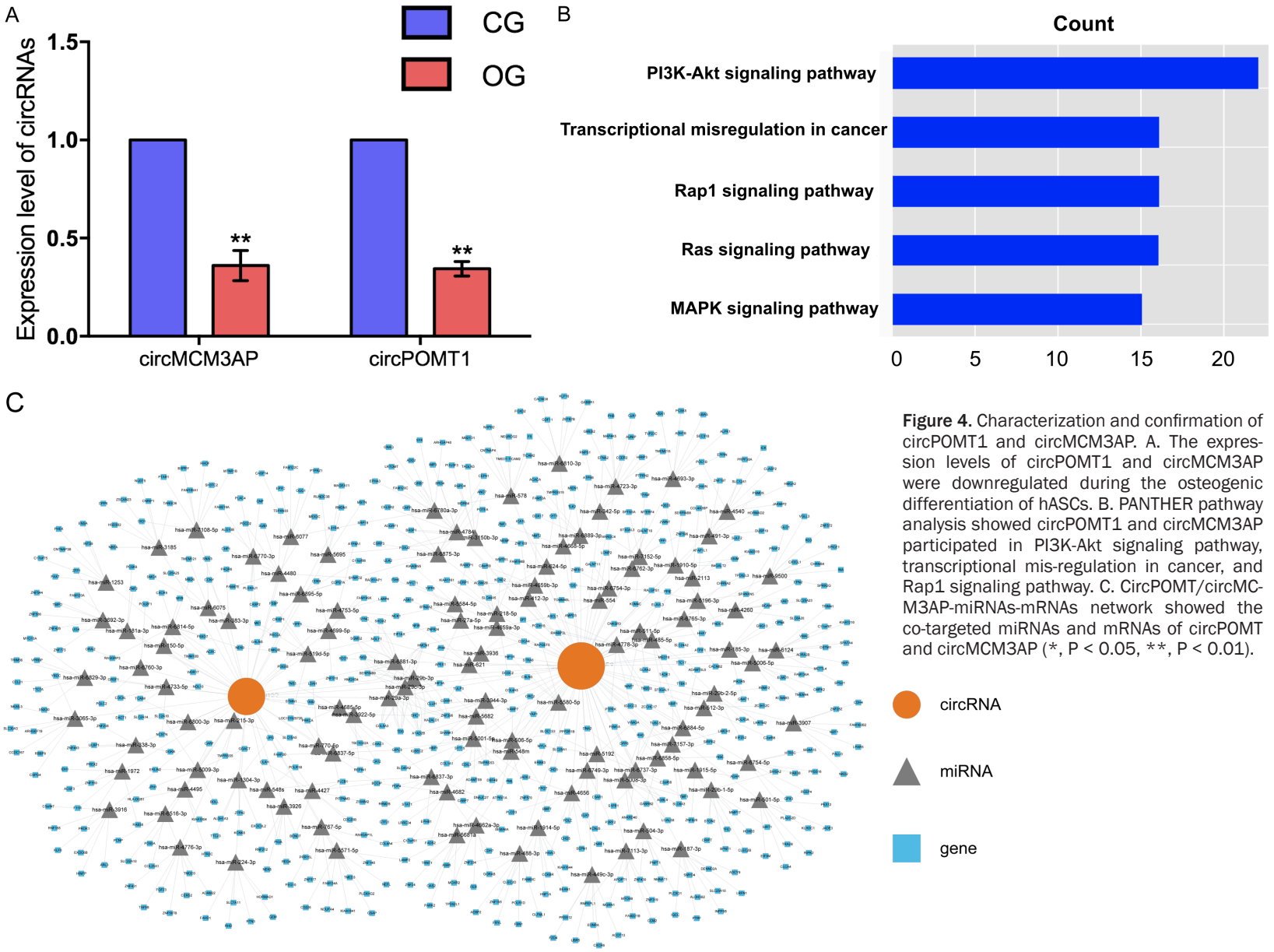

Figure 4. Characterization and confirmation of circPOMT1 and circMCM3AP. A. The expression levels of circPOMT1 and circMCM3AP were downregulated during the osteogenic differentiation of hASCs. B. PANTHER pathway analysis showed circPOMT1 and circMCM3AP participated in PI3K-Akt signaling pathway, transcriptional mis-regulation in cancer, and Rap1 signaling pathway. C. CircPOMT/circMCM3AP-miRNAs-mRNAs network showed the co-targeted miRNAs and mRNAs of circPOMT and circMCM3AP (*, $P < 0.05$, **, $P < 0.01$).

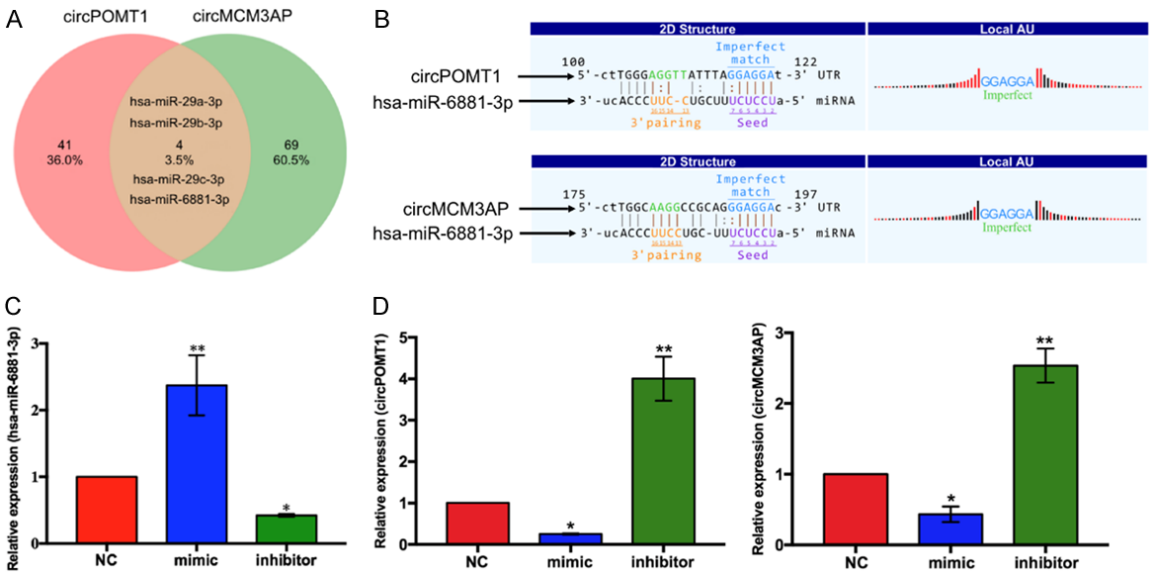

Figure 5. CircPOMT1 and circMCM3AP co-targeted hsa-miR-6881-3p. A. CircPOMT1 and circMCM3AP co-targeted 4 miRNAs. B. There were miRNA-binding sites of hsa-miR-6881-3p in the sequences of circPOMT1 and circMCM3AP respectively. C. Real-time qPCR showed hsa-miR-6881-3p mimic increased the expression of hsa-miR-6881-3p, while hsa-miR-6881-3p inhibitor inhibited the expression of hsa-miR-6881-3p significantly. D. Real-time qPCR showed hsa-miR-6881-3p inhibited the expression of circPOMT1 and circMCM3AP significantly (*, P < 0.05, **, P < 0.01).

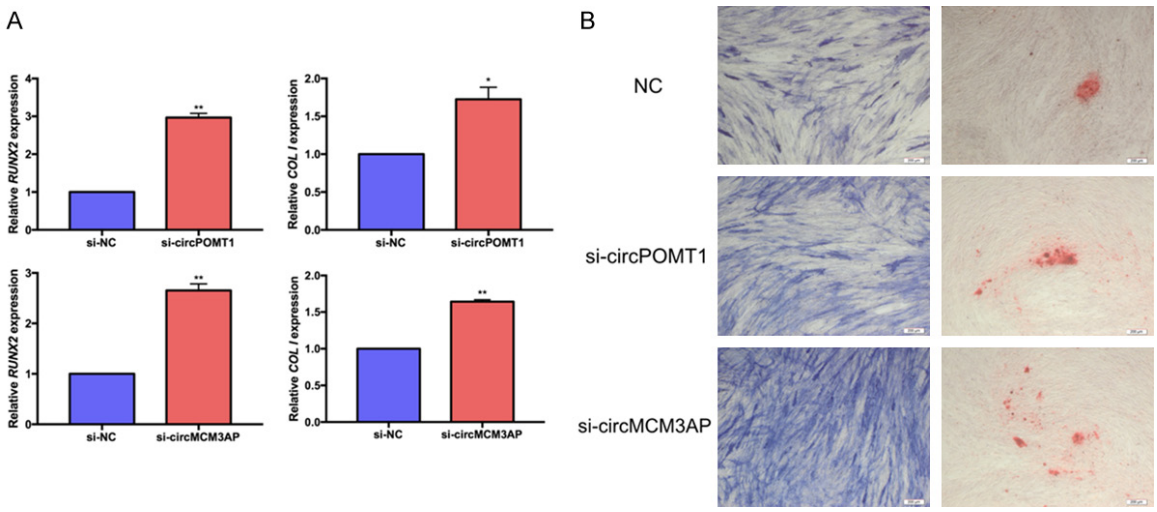

Figure 6. The effects of circPOMT1 and circMCM3AP on the osteogenesis of hASCs. A. Real-time qPCR showed si-circPOMT1 and si-circMCM3AP promoted the expression of RUNX2 and COL I. B. The ALP and ARS staining confirmed si-circPOMT1 and si-circMCM3AP enhanced osteogenic differentiation of hASCs (scale bar = 200 um) (*, P < 0.05, **, P < 0.01).

miRanda, there was one miRNA-binding site of hsa-miR-6881-3p in the sequences of circPOMT1 and circMCM3AP, respectively (**Figure 5B**).

After transfected with hsa-miR-6881-3p mimic and hsa-miR-6881-3p inhibitor for 3 days, the expression level of hsa-miR-6881-3p was increased obviously in hsa-miR-6881-3p mimic group, while it was decreased in hsa-miR-6881-3p inhibitor group significantly, compared to negative control (NC) (**Figure 5C**).

Meanwhile, the expression levels of circPOMT1 and circMCM3AP were downregulated in hsa-miR-6881-3p mimic group respectively, and

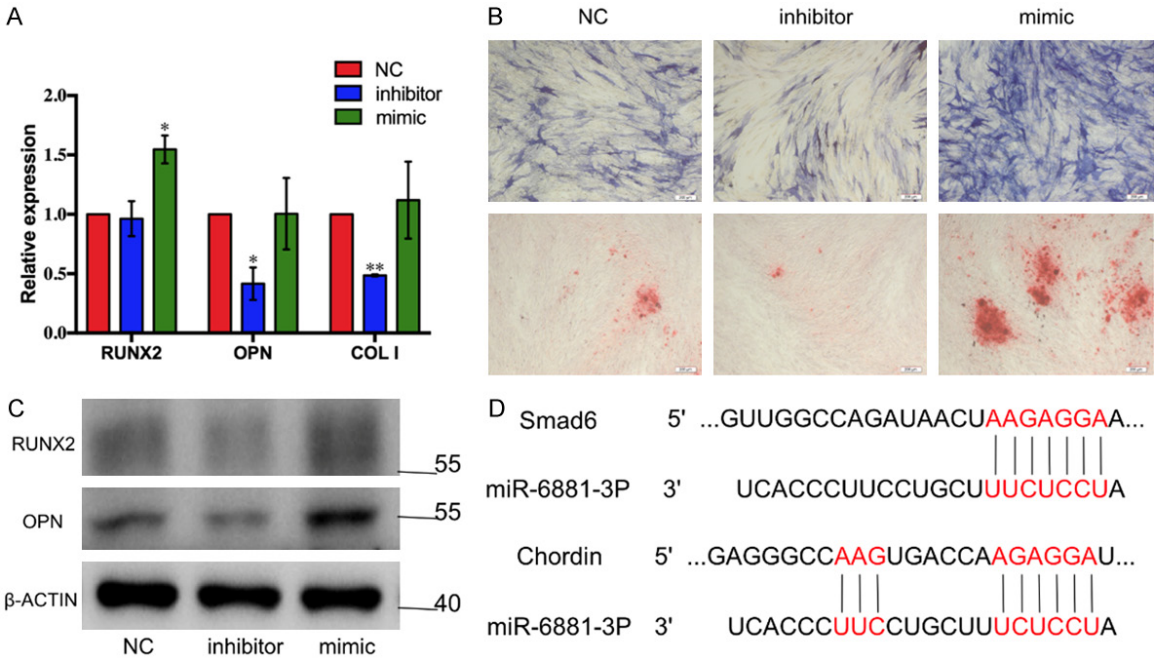

Figure 7. The effects of hsa-miR-6881-3p on the osteogenesis of hASCs. A. Real-time qPCR showed hsa-miR-6881-3p promoted the expression of RUNX2, OPN, and COL I. B. The ALP and ARS staining confirmed hsa-miR-6881-3p mimic enhanced osteogenesis of hASCs, and hsa-miR-6881-3p inhibitor inhibited the osteogenic differentiation of hASCs (scale bar = 200 um). C. hsa-miR-6881-3p promoted the protein expression of RUNX2 and OPN (the numbers on the right side are in kDa). D. There were binding sites of Chordin and Smad6 in the sequence of miR-6881-3p (*, $P < 0.05$, **, $P < 0.01$).

both of the circRNAs were upregulated in hsa-miR-6881-3p inhibitor group (**Figure 5D**), which indicated circPOMT1 and circMCM3AP were negatively related with hsa-miR-6881-3p.

The effects of circPOMT1 and circMCM3AP on the osteogenesis of hASCs

Transfection was performed to knock down the expression of circPOMT1 and circMCM3AP. The results of qRT-PCR indicated that the expression levels of COL I and RUNX2 were increased in both circPOMT1 and circMCM3AP knockdown groups when compared to group NC (**Figure 6A**). After induction for 7 days, the intensity of ALP was significantly stronger and the calcified nodules were more apparent in both circPOMT1 and circMCM3AP knockdown groups than that in group NC (**Figure 6B**).

The effects of hsa-miR-6881-3p on the osteogenesis of hASCs

After transfected hsa-miR-6881-3p mimic for 7 days, the mRNA expression of RUNX2 was increased significantly ($P < 0.05$), while OPN and COL I were upregulated without statistical significance. In hsa-miR-6881-3p inhibitor group, the expression levels of OPN and COL I were decreased significantly ($P < 0.05$, $P < 0.01$, respectively), while RUNX2 was downregulated without statistical significance (**Figure 7A**).

The ALP staining showed that the intensity of ALP was significantly stronger in hsa-miR-6881-3p mimic group than that in group NC, while it was obviously weaker in hsa-miR-6881-3p inhibitor group. The calcified nodules in hsa-miR-6881-3p mimic group were more apparent (**Figure 7B**). These results demonstrated that hsa-miR-6881-3p could enhance the activity of ALP and the calcium deposition.

The protein levels of RUNX2 and OPN were upregulated obviously in hsa-miR-6881-3p mimic group. The expression levels of these two proteins, however, were reduced in hsa-miR-6881-3p inhibitor group (**Figures 7C**, S1, S2 and S3).

According to TargetScanHuman 7.2 database, hsa-miR-6881-3p was predicted to directly target Smad6 and Chordin, which were two critical inhibitors of bone morphogenetic proteins (BMPs) signaling pathway (**Figure 7D**).

Discussion

CircRNAs could influence the splicing of their host genes, directly regulate the protein function, and participate in the translation of protein via cap-independent mechanism, to carry out the biological functions [29]. One of the most important mechanism is that circRNAs contained the binding sites of miRNAs, which enabled the circRNAs to competently bind to miRNAs and serve as miRNAs sponges to weaken or eliminate the inhibitive effect of miRNAs on the target genes. Quite a lot of miRNAs have been suggested to be closely related to osteogenic differentiation of mesenchymal stem cells (MSCs) and the regulation of bone formation [15].

It is reported that circNOTCH3 and circCD59 could regulate the expression of miR-204 and miR-2861 [30] to enhance the expression of RUNX2 and promote osteogenic differentiation of periodontal ligament stem cells (PDLSCs) [31-33]. The co-expressed genes in this process were closely related to the regulation of extracellular matrix mineralization, proliferation of MSCs, and BMPs signaling pathway [30]. CircBANP and circITCH were predicted to target miR-34a and miR-146a, both of which might regulate osteogenic differentiation of PDLSCs through mitogen-activated protein kinases (MAPKs) signaling pathway [34]. In BMP-2-mediated osteogenesis of MC3T3-E1 cells, circ19142 and circ5846 could inhibit the expression of miR-7067-5p to promote osteogenic differentiation of MC3T3-E1 cells [35]. Mm9_circ_009056 could act as the sponge of miR-22-3p during the osteogenesis of MC3T3-E1 cells, which contributed to the activation of Wnt/β-catenin signaling pathway, the regulation of BMP-7 expression, and the promotion of bone formation [36, 37]. However, few studies have focused on the functions and the regulation mechanism of circRNAs in the osteogenesis of hASCs.

In this study, 210 differentially expressed circRNAs were detected by circRNA sequencing during the osteogenesis of hASCs, wherein 150 circRNAs were upregulated and 60 circRNAs were downregulated. The expression of circPOMT1 and circMCM3AP were decreased in OG, which suggested these two circRNAs might restrain the osteogenesis of hASCs. According to PANTHER pathway analysis, circPOMT1 and circMCM3AP had a strong relationship with several classical osteogenic signaling pathways, such as PI3K/Akt signaling pathway. It is reported that PI3K/Akt signaling pathway participated in the cell proliferation, differentiation, invasion, and apoptosis [38], and the activation of PI3K/Akt signaling pathway was necessary for the proliferation and differentiation of osteoblasts in rats [39]. It is indicated that miRNA-21 could promote osteogenesis of bone marrow-derived stem cells (BMSCs) to enhance the bone regeneration in critical size defects via the PI3K/Akt pathway [40]. Additionally, we identified the binding sites of hsa-miR-6881-3p in the sequences of both circPOMT1 and circMCM3AP, and the expression of hsa-miR-6881-3p was negatively correlated with circPOMT1 and circMCM3AP, indicating that circPOMT1 and circMCM3AP might regulate the osteogenic differentiation of hASCs by targeting hsa-miR-6881-3p.

It is suggested that hsa-miR-6881-3p could promote the osteogenesis of hASCs in this study. hsa-miR-6881-3p was reported to be involved in the p53-mediated ceRNAs network [41]. It was well established that p53 played an inhibitory role in the osteogenic differentiation by mouse genetics and cell-based approaches [42]. Previous studies showed that p53 could block RUNX2 transcriptional activity [43], and could prevent osterix from binding to the Sp1/GC-rich sequences [44]. p53 deletion could result in the expression changes of Smad1 and Smurf1 [45], which allowed the overactivation of BMPs signaling pathway.

According to the results of the TargetScanHuman 7.2, hsa-miR-6881-3p could also directly bind to Smad6 and Chordin, which were critical check points of BMPs signaling pathway. BMPs are multifunctional growth factors transducing signals through Smads-dependent and non-Smads-dependent pathways to play biological roles. BMP ligands could bind to type I (BMPR-I) and type II receptors (BMPR-II), which triggered the phosphorylation of the R-Smad1/5/8. Phosphorylated R-Smads formed a heteromeric complex with the co-Smad4 and subsequently translocated to the nucleus, which promoted the targeted genes, such as RUNX2 and osterix, to transcript [46]. Chordin could be bound to BMP ligands to prevent the ligand-receptor interaction and thus inhibit the signal transduction [47]. Smad6 could inhibit the formation of R-Smads and co-Smad4 complexes and serve

as an endogenous inhibitor of BMPs signaling pathway [48]. Therefore, it is suggested hsa-miR-6881-3p might inhibit Smad6 and Chordin to activate BMPs signaling pathway and promote osteogenesis of hASCs.

In summary, the present study identified two novel circRNAs, namely circPOMT1 and circMCM3AP, which could crosstalk with hsa-miR-6881-3p to influence the osteogenesis of hASCs via BMPs signaling pathway. CircPOMT1 and circMCM3AP are potential targets for bone regeneration of critical bone defects.

Acknowledgements

This study was supported by grants from the National Natural Science Foundation of China (81771048, 81870743 and 81470722) and the Creative Spark Fund of Sichuan University (2018SCUH0007).

Disclosure of conflict of interest

None.

Address correspondence to: Jun Liu and Zhi-He Zhao, State Key Laboratory of Oral Diseases & National Clinical Research Center for Oral Diseases, West China Hospital of Stomatology, Sichuan University, No. 14, 3rd Section, South Renmin Road, Chengdu 610041, Sichuan, China. E-mail: junliu@scu.edu.cn (JL); zhzhao@scu.edu.cn (ZHZ)

References

[1] Cancedda R, Giannoni P and Mastrogiacomo M. A tissue engineering approach to bone repair in large animal models and in clinical practice. Biomaterials 2007; 28: 4240-4250.

[2] Roseti L, Parisi V, Petretta M, Cavallo C, Desando G, Bartolotti I and Grigolo B. Scaffolds for bone tissue engineering: state of the art and new perspectives. Mater Sci Eng C Mater Biol Appl 2017; 78: 1246-1262.

[3] Frese L, Dijkman PE and Hoerstrup SP. Adipose tissue-derived stem cells in regenerative medicine. Transfus Med Hemother 2016; 43: 268-274.

[4] Kokai LE, Marra K and Rubin JP. Adipose stem cells: biology and clinical applications for tissue repair and regeneration. Transl Res 2014; 163: 399-408.

[5] Sándor GK, Numminen J, Wolff J, Thesleff T, Miettinen A, Tuovinen VJ, Mannerström B, Patrikoski M, Seppänen R, Miettinen S, Rautiainen M and Öhman J. Adipose stem cells used to reconstruct 13 cases with cranio-maxillofacial hard-tissue defects. Stem Cells Transl Med 2014; 3: 530-40.

[6] Saxer F, Scherberich A, Todorov A, Studer P, Miot S, Schreiner S, Güven S, Tchang LA, Haug M, Heberer M, Schaefer DJ, Rikli D, Martin I and Jakob M. Implantation of stromal vascular fraction progenitors at bone fracture sites: from a rat model to a first-in-man study. Stem Cells 2016; 34: 2956-2966.

[7] Gelberman RH, Shen H, Kormpakis I, Rothrauff B, Yang G, Tuan RS, Xia Y, Sakiyama-Elbert S, Silva MJ and Thomopoulos S. Effect of adipose-derived stromal cells and BMP12 on intrasynovial tendon repair: a biomechanical, biochemical, and proteomics study. J Orthop Res 2015; 34: 630-640.

[8] Tapp H, Hanley EN, Patt JC and Gruber HE. Adipose-derived stem cells: characterization and current application in orthopaedic tissue repair. Exp Biol Med (Maywood) 2009; 234: 1-9.

[9] Wilusz JE and Sharp PA. A Circuitous route to noncoding RNA. Science 2013; 340: 440-441.

[10] Li X, Yang L and Chen LL. The biogenesis, functions, and challenges of circular RNAs. Mol Cell 2018; 71: 428-442.

[11] Qu S, Yang X, Li X, Wang J, Gao Y, Shang R, Sun W, Dou K and Li H. Circular RNA: a new star of noncoding RNAs. Cancer Lett 2015; 365: 141-148.

[12] Zhang XO, Wang HB, Zhang Y, Lu X, Chen LL and Yang L. Complementary sequence-mediated exon circularization. Cell 2014; 159: 134-147.

[13] Panda AC, Grammatikakis I, Munk R, Gorospe M and Abdelmohsen K. Emerging roles and context of circular RNAs. Wiley Interdiscip Rev RNA 2016; 8.

[14] Hansen TB, Jensen TI, Clausen BH, Bramsen JB, Finsen B, Damgaard CK and Kjems J. Natural RNA circles function as efficient microRNA sponges. Nature 2013; 495: 384-388.

[15] Chen C and Sarnow P. Initiation of protein synthesis by the eukaryotic translational apparatus on circular RNAs. Science 1995; 268: 415-417.

[16] Guo JU, Agarwal V, Guo H and Bartel DP. Expanded identification and characterization of mammalian circular RNAs. Genome Biol 2014; 15: 409.

[17] Li J, Yang J, Zhou P, Le Y, Zhou C, Wang S, Xu D, Lin HK and Gong Z. Circular RNAs in cancer: novel insights into origins, properties, functions and implications. Am J Cancer Res 2015; 5: 472-480.

[18] Salzman J, Gawad C, Wang PL, Lacayo N and Brown PO. Circular RNAs are the predominant transcript isoform from hundreds of human genes in diverse cell types. PLoS One 2012; 7: e30733.

[19] Memczak S, Jens M, Elefsinioti A, Torti F, Krueger J, Rybak A, Maier L, Mackowiak SD,

Gregersen LH, Munschauer M, Loewer A, Ziebold U, Landthaler M, Kocks C, le Noble F and Rajewsky N. Circular RNAs are a large class of animal RNAs with regulatory potency. Nature 2013; 495: 333-338.

[20] Nitsche A, Doose G, Tafer H, Robinson M, Saha NR, Gerdol M, Canapa A, Hoffmann S, Amemiya CT and Stadler PF. Atypical RNAs in the coelacanth transcriptome. J Exp Zool B Mol Dev Evol 2014; 322: 342-51.

[21] Suzuki H, Zuo Y, Wang J, Zhang MQ, Malhotra A and Mayeda A. Characterization of RNase R-digested cellular RNA source that consists of lariat and circular RNAs from pre-mRNA splicing. Nucleic Acids Res 2006; 34: e63.

[22] Karreth FA, Tay Y, Perna D, Ala U, Tan SM, Rust AG, DeNicola G, Webster KA, Weiss D, Perez-Mancera PA, Krauthammer M, Halaban R, Provero P, Adams DJ, Tuveson DA and Pandolfi PP. In vivo identification of tumor-uppressive PTEN ceRNAs in an oncogenic BRAF-induced mouse model of melanoma. Cell 2011; 147: 382-395.

[23] Van Rossum D, Verheijen BM and Pasterkamp RJ. Circular RNAs: novel regulators of neuronal development. Front Mol Neurosci 2016; 9: 74.

[24] Meng S, Zhou H, Feng Z, Xu Z, Tang Y, Li P and Wu M. CircRNA: functions and properties of a novel potential biomarker for cancer. Mol cancer 2017; 16: 94.

[25] Yang ZG, Awan FM, Du WW, Zeng Y, Lyu J, Wu, Gupta S, Yang W and Yang BB. The circular RNA interacts with STAT3, increasing its nuclear translocation and wound repair by modulating dnmt3a and miR-17 function. Mol Ther 2017; 25: 2062-2074.

[26] Li L, Guo J, Chen Y, Chang C and Xu C. Comprehensive circRNA expression profile and selection of key circRNAs during priming phase of rat liver regeneration. BMC Genomics 2017; 18: 80.

[27] Alhasan AA, Izuogu OG, Al-Balool HH, Steyn JS, Evans A, Colzani M, Ghevaert C, Mountford JC, Marenah L, Elliott DJ, Santibanez-Koref M and Jackson MS. Circular RNA enrichment in platelets is a signature of transcriptome degradation. Blood 2016; 127: e1-e11.

[28] Du WW, Yang W, Chen Y, Wu ZK, Foster FS, Yang Z, Li X and Yang BB. Foxo3 circular RNA promotes cardiac senescence by modulating multiple factors associated with stress and senescence responses. Eur Heart J 2017; 38: 1402-1412.

[29] Greco S, Cardinali B, Falcone G and Martelli F. Circular RNAs in muscle function and disease. Int J Mol Sci 2018; 19: E3454.

[30] Zheng Y, Li X, Huang Y, Jia L and Li W. The Circular RNA landscape of periodontal ligament stem cells during osteogenesis. J Periodont 2017; 88: 906-914.

[31] Huang J, Zhao L, Xing L and Chen D. MicroRNA-204 regulates Runx2 protein expression and mesenchymal progenitor cell differentiation. Stem Cells 2010; 28: 357-364.

[32] Diomede F, Merciaro I, Martinotti S, Cavalcanti MF, Caputi S, Mazzon E and Trubiani O. miR-2861 is involved in osteogenic commitment of human periodontal ligament stem cells grown onto 3D scaffold. J Biol Regul Homeost Agents 2016; 30: 1009-1018.

[33] Xia ZY, Hu Y, Xie PL, Tang SY, Luo XH, Liao EY, Chen F and Xie H. Runx2/miR-3960/miR-2861 positive feedback loop Is responsible for osteogenic transdifferentiation of vascular smooth muscle cells. Biomed Res Int 2015; 2015: 624037.

[34] Gu X, Li M, Jin Y, Liu D and Wei F. Identification and integrated analysis of differentially expressed lncRNAs and circRNAs reveal the potential ceRNA networks during PDLSC osteogenic differentiation. BMC Genet 2017; 18: 100.

[35] Qian DY, Yan GB, Bai B, Chen Y, Zhang SJ, Yao YC and Xia H. Differential circRNA expression profiles during the BMP2-induced osteogenic differentiation of MC3T3-E1 cells. Biomed Pharmacother 2017; 90: 492-499.

[36] Wu C, Zheng Z, Ren W, Deng T, Li Y, Yang L, Wu J, Huang Z, Li Z and Guo L. Mm9_circ_009056 enhances osteogenesis by targeting BMP7 via CGRP-mediated miR-22-3p. Biochem Biophys Res Commun 2018; 501: 199-205.

[37] Gong YY, Peng MY, Yin DQ and Yang YF. Long non-coding RNA H19 promotes the osteogenic differentiation of rat ectomesenchymal stem cells via Wnt/β-catenin signaling pathway. Eur Rev Med Pharmacol Sci 2018; 22: 8805-8813.

[38] Ma P, Gu B, Xiong W, Tan B, Geng W, Li J and Liu H. Glimepiride promotes osteogenic differentiation in rat osteoblasts via the PI3K/Akt/eNOS pathway in a high glucose microenvironment. PLoS One 2014; 9: e112243.

[39] Ma P, Gu B, Ma J, E L, Wu X, Cao J, Liu H. Glimepiride induces proliferation and differentiation of rat osteoblasts via the PI3-kinase/Akt pathway. Metabolism 2010; 59: 359-366.

[40] Yang C, Liu X, Zhao K, Zhu Y, Hu B, Zhou Y, Wang M, Wu Y, Zhang C, Xu J, Ning Y and Zou D. miRNA-21 promotes osteogenesis via the PTEN/PI3K/Akt/HIF-1α pathway and enhances bone regeneration in critical size defects. Stem Cell Res Ther 2019; 10: 65.

[41] Zhang Y, Kang R, Liu W, Yang Y, Ding R, Huang Q, Meng J, Xiong L and Guo Z. Identification and analysis of P53-mediated competing endogenous RNA network in human hepatocellular carcinoma. Int J Biol Sci 2017; 13: 1213-1221.

[42] He Y, de Castro LF, Shin MH, Dubois W, Yang HH, Jiang S, Mishra PJ, Ren L, Gou H, Lal A, Khanna C, Merlino G, Lee M, Robey PG and Huang J. p53 loss increases the osteogenic differentiation of bone marrow stromal cells. Stem Cells 2015; 33: 1304-1319.

[43] van der Deen M, Taipaleenmäki H, Zhang Y, Teplyuk NM, Gupta A, Cinghu S, Shogren K, Maran A, Yaszemski MJ, Ling L, Cool SM, Leong DT, Dierkes C, Zustin J, Salto-Tellez M, Ito Y, Bae SC, Zielenska M, Squire JA, Lian JB, Stein JL, Zambetti GP, Jones SN, Galindo M, Hesse E, Stein GS and van Wijnen AJ. MicroRNA-34c inversely couples the biological functions of the runt-related transcription factor RUNX2 and the tumor suppressor p53 in osteosarcoma. J Biol Chem 2013; 288: 21307-21319.

[44] Artigas N, Gámez B, Cubillos-Rojas M, Sánchez-de Diego C, Valer JA, Pons G, Rosa JL and Ventura F. P53 inhibits SP7/Osterix activity in the transcriptional program of osteoblast differentiation. Cell Death Differ 2017; 24: 2022-2031.

[45] Ruan X, Zuo Q, Jia H, Chau J, Lin J, Ao J, Xia X, Liu H, Habib SL, Fu C and Li B. P53 deficiency-induced Smad1 upregulation suppresses tumorigenesis and causes chemoresistance in colorectal cancers. J Mol Cell Biol 2015; 7: 105-118.

[46] Zhang X, Guo J, Zhou Y and Wu G. The roles of bone morphogenetic proteins and their signaling in the osteogenesis of adipose-derived stem cells. Tissue Eng Part B Rev 2013; 20: 84-92.

[47] Ali IH and Brazil DP. Bone morphogenetic proteins and their antagonists: current and emerging clinical uses. Br J Pharmacol 2014; 171: 3620-3632.

[48] Hata A, Lagna G, Massagué J and Hemmati-Brivanlou A. Smad6 inhibits BMP/Smad1 signaling by specifically competing with the Smad4 tumor suppressor. Genes Dev 1998; 12: 186-97.

Table S1. The sequences of the RNA oligoribonucleotide

	Primer sequence
hsa-miR-6881-3p mimic	AUCCUCUUUCGUCCUUCCCACU
hsa-miR-6881-3p inhibitor	UAGGAGAAAGCAGGAAGGGUGA
miR-NC	Forward: 5'-UUGUACUACACAAAAGUACUG-3'
si-circPOMT1-1	Forward: 5'-UUGGAGCAGUUUUGACGAATT-3' Reverse: 5'-UUCGUCAAAACUGCUCCAATT-3'
si-circPOMT1-2	Forward: 5'-UGGAGCAGUUUUGACGAAGTT-3' Reverse: 5'-CUUCGUCAAAACUGCUCCATT-3'
si-circPOMT1-3	Forward: 5'-AAUUGGAGCAGUUUUGACGTT-3' Reverse: 5'-CGUCAAAACUGCUCCAAUUTT-3'
si-circMCM3AP-1	Forward: 5'-UAAUUUAAGUUUGGGUGAATT-3' Reverse: 5'-UUCACCCAAACUUAAAUUATT-3'
si-circMCM3AP-2	Forward: 5'-AUUAAUUUAAGUUUGGGUGTT-3' Reverse: 5'-CACCCAAACUUAAAUUAAUTT-3'
si-circMCM3AP-3	Forward: 5'-UAUUAAUUUAAGUUUGGGUTT-3' Reverse: 5'-ACCCAAACUUAAAUUAAUATT-3'
si-NC	Forward: 5'-UUCUCCGAACGUGUCACGUTT-3' Reverse: 5'-ACGUGACACGUUCGGAGAATT-3'

Table S2. The primers list of qRT-PCR

Gene	Primer sequence
circTIPARP	Forward: 5'-ACCTGGCTGCAGTGGAAG-3' Reverse: 3'-GGGTCGGCTTCCATTTTT-5'
circZBTB16	Forward: 5'-AGAGCAGTGCAGCGTGTG-3' Reverse: 3'-CAGATCCATGGTGCTCCC-5'
circXLOC_007414	Forward: 5'-TGATCCTCCCACCTCAGC-3' Reverse: 3'-ACTGTGCTTCTGCCTGGG-5'
circUSP53	Forward: 5'-CGTAGCTGTGGAGCATCG-3' Reverse: 3'-TTTTCATTCCTCCTTGGCA-5'
circPOMT1	Forward: 5'-GCTGGCCTTGGGAGGTTA-3' Reverse: 3'-GGCCCACTGTCATCCAAG-5'
circMCM3AP	Forward: 5'-CCTTTCAGGAAGGAGCCA-3' Reverse: 3'-TCCAGCATCTGCAGGACA-5'
RUNX2	Forward: 5'-CTACTATGGCACTTCGTCAGGAT-3' Reverse: 3'-ATCAGCGTCAACACCATCATT-5'
OPN	Forward: 5'-GGCTAAACCCTGACCCATCTC-3' Reverse: 3'-GTCAATGGAGTCCTGGCTGTC-5'
COL I	Forward: 5'-CCAAGACGAAGACATCCCACCA-3' Reverse: 3'-CCGTTGTCGCAGACGCAGAT-5'
β-ACTIN	Forward: 5'-GTGGCCGAGGACTTTGATTG-3' Reverse: 3'-CCTGTAACAACGCATCTCATATT-5'

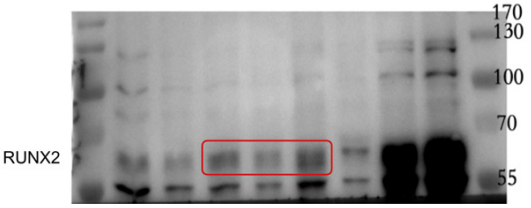

Figure S1. The original western images of RUNX2.

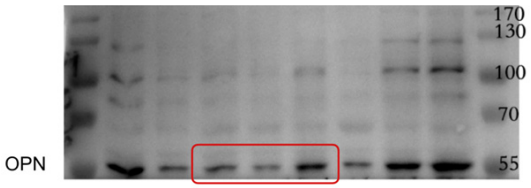

Figure S2. The original western images of OPN.

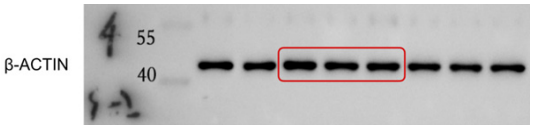

Figure S3. The original western images of β-ACTIN.